

# Geologic Remote Sensing

Alexander F. H. Goetz and Lawrence C. Rowan

Remote sensing refers to all the arts and techniques of measurement and interpretation of phenomena from afar. This article deals specifically with the use of electromagnetic radiation to obtain data about the nature of the surface of the earth. Geologic remote-sensing experiments were initiated nearly two decades ago by a relatively small group of specialists, but acquisition of the first

sources. With remote-sensing techniques it is possible to obtain certain structural and lithologic information more efficiently than can be achieved on the ground. These techniques also facilitate the overall interpretation. In well-exposed, poorly understood areas, reconnaissance geologic maps can be compiled from Landsat images when only limited field information is available (2),

---

**Summary.** Remote-sensing techniques are now being used routinely in geologic interpretation for mineral and energy exploration, plant siting, waste disposal, and the development of models for regional and continental tectonics. New spaceborne methods and associated technologies are being developed to produce data from which geologic information about large areas can be derived much more rapidly than by conventional techniques.

---

multispectral digital data set from orbit in 1972 by the Landsat (1) Multispectral Scanner (MSS) attracted the attention of the entire geologic community. Landsat MSS data are now being applied to a wide variety of specific geologic problems that are difficult to solve by conventional methods alone, including mineral and energy resource exploration, nuclear plant siting and waste disposal, and the charting of glaciers and shallow seas.

A broader, more fundamental application of remote sensing is in the augmentation of conventional methods for compiling and interpreting geologic maps of large regions, because regional geologic maps present compositional, structural, and chronological information essential for reconstructing the geologic evolution. These reconstructions, aided by geophysical data for defining subsurface configurations, are important to all practical applications, because the conditions of formation of rock units and structural features influence, among others, the occurrence of ore and petroleum deposits and the thickness and structural integrity of disposal media.

Geologic maps incorporate a large, varied body of specific field and laboratory measurements, but they are in part interpretative because field measurements are always limited by rock exposure, accessibility, and manpower re-

sources. With remote-sensing techniques it is possible to obtain certain structural and lithologic information more efficiently than can be achieved on the ground. These techniques also facilitate the overall interpretation. In well-exposed, poorly understood areas, reconnaissance geologic maps can be compiled from Landsat images when only limited field information is available (2), because many of the major structural and lithologic elements are well displayed. However, remote sensing can also contribute to a better understanding of areas where considerable detailed geologic mapping is already available. Detailed geologic mapping is generally conducted in small areas, and the continuity of some regional features that have intermittent, variable expressions is often not recognized. Some of these features were first seen in the synoptic views of Landsat images, and some rock units can be mapped much more efficiently if Landsat images are used. However, some critical information cannot be obtained through remote sensing, and the characteristics of the Landsat MSS impose several important limitations on the acquisition of diagnostic lithologic and structural information. Continued research based on the use of laboratory, field, and aircraft data indicates that most of these limitations can be overcome by the design of satellite systems for geologic purposes. Remote-sensing data can make important contributions to the solution of geologic problems. However, in order to be most effective, these data must be used along with geologic mapping in the field as well as geophysical and geochemical surveys.

In this article we describe the basis for terrestrial remote-sensing techniques,

using the analysis of spectral reflectance, spectral emittance, thermal inertia, and radar. Several specific applications of Landsat MSS data are discussed with emphasis on those dealing with mineral exploration. Geologic mapping with the aid of satellite data entails the description of structure, lithologic units, and geobotanical relationships. The results of recent aircraft experiments are discussed to illustrate the potential of satellite systems for more detailed lithologic mapping. An entirely comprehensive review is not attempted, but key references are given to form the basis for more thorough consideration.

## Physical Basis of Remote-Sensing Techniques

The wavelengths of interest for remote sensing (Fig. 1) extend from the ultraviolet, at about 0.4 micrometer, to microwaves, at 50 centimeters, a wavelength range of  $10^6$ . The data are generally obtained from the upper micrometers or millimeters of the surface because of the high opacity and scattering characteristics of natural materials. The opacity in the visible and infrared portions of the spectrum is created by high absorption coefficients due to a variety of electronic and vibrational processes (3, 4). In the microwave region, high conductivity and dielectric constant caused by the presence of water restrict penetration (5). Some information concerning body properties as opposed to surface properties can be obtained if one analyzes the changes in surface temperature that are induced by diurnal solar heating. This property, called thermal inertia, is defined as  $(k\rho c)^{1/2}$ , where  $k$  is the thermal conductivity,  $\rho$  is the density, and  $c$  is the specific heat (6). Even this method allows measurement to a depth of only about 10 cm or less.

For ease of reference, the spectrum can be divided into several distinct segments: ultraviolet, visible and near-infrared, short-wavelength infrared, mid-infrared, and microwave. The ultraviolet wavelengths, below  $0.4 \mu\text{m}$ , are generally not exploited for orbital remote sensing because of high atmospheric absorption and Rayleigh scattering. The spectral reflectance of minerals in the visible and near-infrared, extending to  $1.0 \mu\text{m}$ , is influenced mainly by the wings of charge transfer bands in the ultraviolet and electronic transitions in the visible

---

Dr. Goetz is a senior member of the technical staff of the Jet Propulsion Laboratory, California Institute of Technology, Pasadena 91109. Dr. Rowan is a geologist with the U.S. Geological Survey, Reston, Virginia 22092.

and near-infrared (7) that occur in the transition elements. On the earth's surface, iron is the most common transition element. The most important spectral features in this wavelength region are the steep falloff of reflectance in the visible toward the ultraviolet and an absorption band between 0.85 and 0.92  $\mu\text{m}$  associated with the  $\text{Fe}^{3+}$  electronic transition (Fig. 2, curve 2 or 3). These spectral features are characteristic of iron oxides and hydrous iron oxides, collectively referred to as limonite, and have made it possible to identify and map limonitic alteration zones that are important surface indicators used in exploration for precious and base metals.

The short-wavelength infrared region, 1 to 3  $\mu\text{m}$ , provides more diagnostic

spectral information about the composition of minerals and rocks than the visible and near-infrared regions. Absorption bands at 1.4 and 1.9  $\mu\text{m}$  are caused by the bound and unbound water contained in surface materials. Unfortunately, these bands (Fig. 2) coincide with strong atmospheric water bands (Fig. 1) that render the atmosphere opaque for all but the highest topographic elevations.

The region around 1.6  $\mu\text{m}$  exhibits the highest reflectance for most rocks because it is nearly midway between the ultraviolet-visible iron absorption bands and a strong fundamental  $\text{OH}^-$  vibration at 2.74  $\mu\text{m}$ . In particular, altered rocks (8) containing clay with or without a short-wavelength  $\text{Fe}^{3+}$  absorption, ex-

hibit a pronounced peak reflectance (Fig. 2), often greater than 70 percent, at 1.6  $\mu\text{m}$  (9). The region from 2 to 2.5  $\mu\text{m}$  is of particular interest because it contains sharp, highly diagnostic spectral absorption bands caused by lattice overtone bending-stretching vibrations for layered silicates (10), such as clays and micas, and for carbonates (Fig. 2).

Vegetation covers much of the surface of the earth and therefore must be considered in most practical remote-sensing applications. The spectral reflectance of vegetation in the visible and near-infrared regions differs markedly from that of rock and soils (Fig. 2). This spectral region contains the intense chlorophyll absorption and the region of high reflectance beyond 0.7  $\mu\text{m}$ . The large differences in spectral reflectance between vegetation and rocks means that even a small amount of vegetation will alter the apparent spectral signatures of rocks and soils. In particular, the recognition of limonite is made difficult because the diagnostic slope of the reflectance curve in the visible and the absorption band near 0.87  $\mu\text{m}$  is masked by the high reflectance of vegetation. On the other hand, as discussed below, subtle variations in the spectrum of stressed vegetation have been used to outline mineralized areas. Moreover, the regional distribution of vegetation can be used in some areas as an indirect indicator of the composition of the soil beneath.

The emissive portion of the spectrum available for terrestrial observation, called the mid-infrared, extends from 3 to 15  $\mu\text{m}$ . The region from 3 to 5  $\mu\text{m}$  contains diagnostic spectral bands for nitrates and sulfates (11). However, this spectral region has not been thoroughly investigated for use as an identifier of surface material because of the low energy flux available from the surface and because the crossover point between solar-reflected and surface-emitted energy occurs here.

The mid-infrared region beyond 8  $\mu\text{m}$  is especially important for geologic mapping because spectral emittance variations provide a basis for distinguishing between silicate and nonsilicate rocks and for discriminating among silicate rocks. Moreover, important distinctions not apparent in multispectral mid-infrared data or in the visible and near-infrared regions, can be discerned from differences in the thermal inertia. These two techniques can be used together to provide considerable fundamental lithologic information.

In the region from 8 to 14  $\mu\text{m}$ , manifestations of the fundamental Si-O stretch-

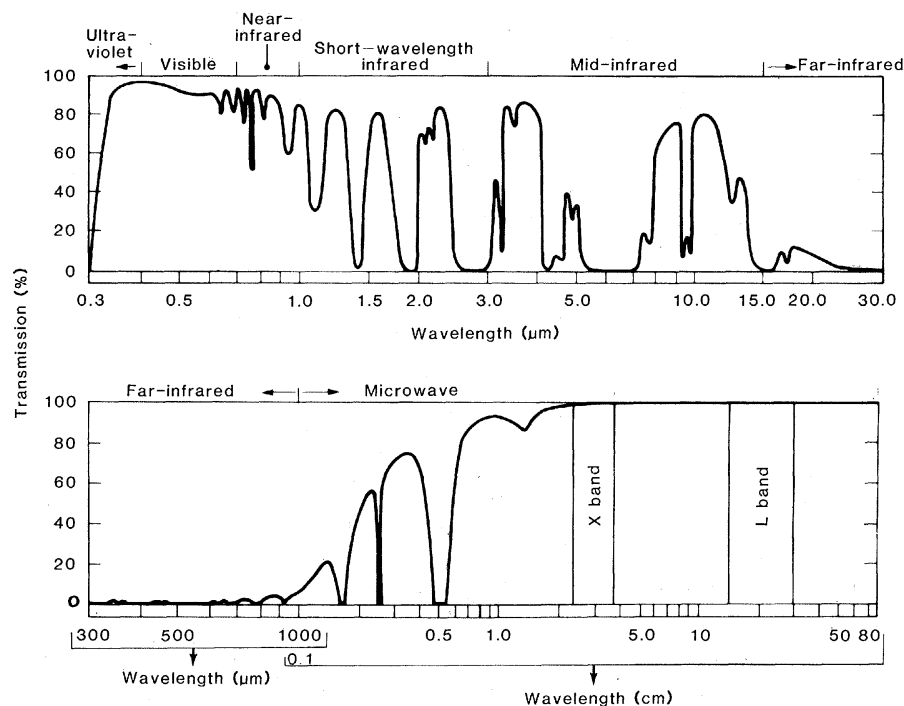


Fig. 1. Generalized absorption spectrum of the atmosphere at the zenith with the named spectral regions outlined.

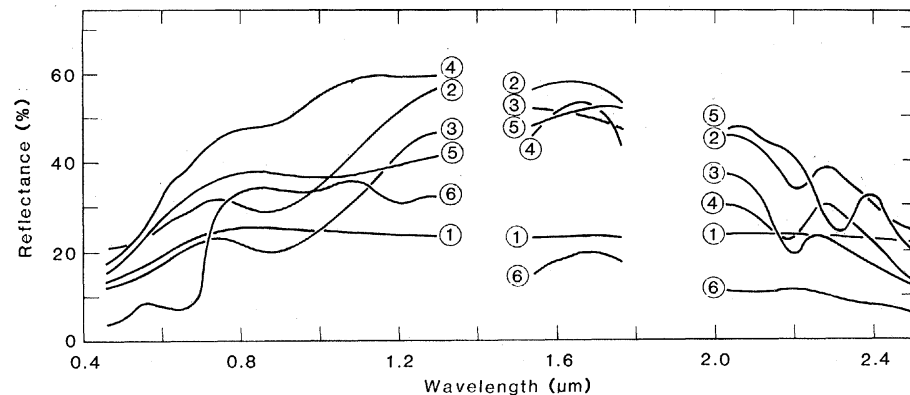


Fig. 2. Field-acquired reflectance spectra: 1, unaltered tuff fragments and soil; 2, argillized andesite fragments; 3, silicified dacite; 4, opaline tuff; 5, tan marble; 6, ponderosa pine. The gaps at 1.4 and 1.9  $\mu\text{m}$  are the result of atmospheric water absorption.

ing vibration are diagnostic of the major types of silicates (12, 13) (Fig. 3). The position of the reststrahlen bands or regions of metallic-like reflection are dependent on the extent of interconnection of the Si-O tetrahedra comprising the crystal lattice. The end-members are represented by quartz, with complete sharing of the oxygen molecules, to olivine, which consists of isolated SiO<sub>4</sub> tetrahedra. The spectral emittance of silicate rocks is especially sensitive to variations in the quartz content (14). In the far-infrared region, 15 to 1000 μm, diagnostic silicate spectral bands are present but the terrestrial atmosphere is essentially opaque.

Emission in the millimeter and centimeter wavelength regions, the microwave region, has not proved useful for direct lithologic discrimination although effects of subsurface layering have been observed (15). However, active microwave systems such as radar imagers in these wavelength regions have proved

effective in structural interpretation, particularly in areas of persistent cloud cover (16). Airborne X-band (3 cm) radar images are now widely used for interpretation in heavily vegetated areas and in areas of low relief. At X band, most surface materials appear uniformly rough so that disturbing cultural and vegetation density effects are minimized, unmasking subtle topographic expression. The low apparent illumination angles available from airborne radar systems also enhance subtle relief, which is particularly important where low-sun-angle photographs cannot be obtained.

Longer wavelength radar, such as L band (25 cm), is more sensitive to surface roughness scales found in nature. The use of the backscatter properties of surface materials to determine material type is being actively investigated (17), and these studies will shape the nature of future active microwave systems for geologic remote sensing.

#### Data Acquisition and Processing

Prior to the mid-1960's, remote sensing was limited to the interpretation of film images. The development of optomechanical scanner systems was important because digital multispectral images could then be constructed at wavelengths outside the sensitivity of range of film. Landsat MSS images are the best known products of these systems (1).

Landsat was followed by several orbital systems that also acquired digital data of interest to geologists: Skylab experiment S-192, a 13-channel multispectral imager (18); Seasat synthetic aperture L-band radar (19); and the Heat Capacity Mapping Mission (HCMM), providing day-night thermal and visible images for mapping the thermal inertia of surface materials (20).

With the advent of Landsat, digital image processing became necessary in order to exploit fully the spectral, spatial, and temporal content of the data. The

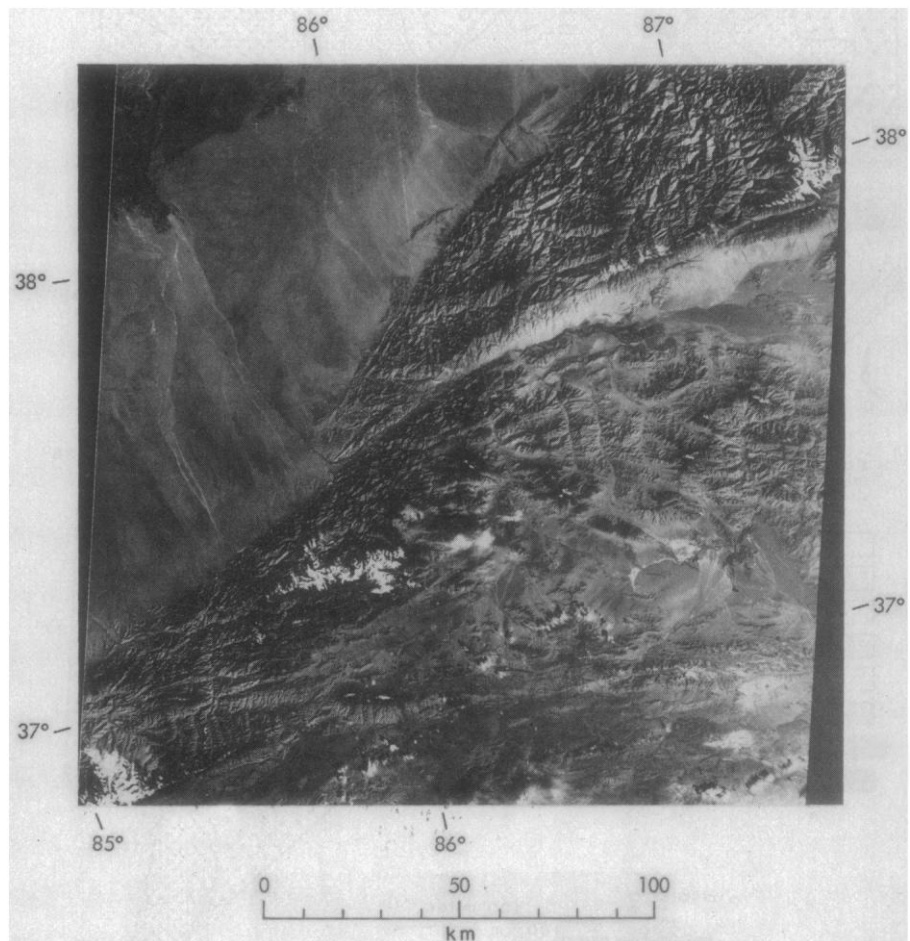
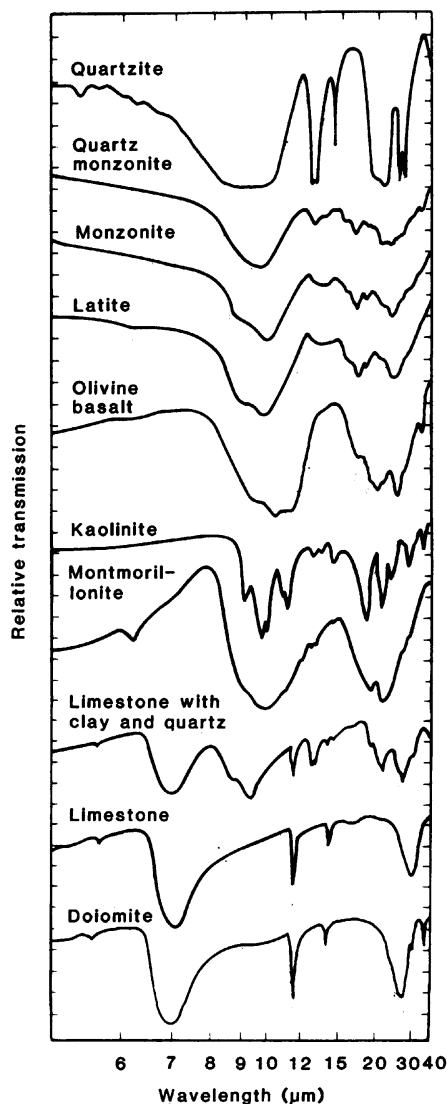


Fig. 3 (left). Transmission spectra of some common silicates (12). Regions of low transmission are associated with reststrahlen bands and are equivalent to regions of low emittance. Fig. 4 (right). Landsat MSS image showing the Altun Shan strike-slip fault zone separating the Tarim Basin in the north from the mountains of Tibet in the south (28).

subject of image processing is far too large to be treated here (21), but some specific methods presently being applied to images for geologic analysis are worth describing.

Instruments such as the Landsat MSS provide multiple, spatially registered data sets, each taken at a different wavelength. The advantage of digital over photographic processing is that transformations applied to the data are precisely known and repeatable and are not subject to the vagaries of complex and often difficult to control chemical processing (22). With digital processing, it is possible to manipulate and combine a large

number of spectral images or other types of data sets.

Digital processing techniques applicable to geologic problems include contrast enhancement, spatial filtering to enhance morphological or structural information, and arithmetic operations such as ratioing of spectral bands to enhance spectral reflectance differences and suppress systematic effects such as topography. Statistical analysis is used to reduce dimensionality in data sets containing many spectral bands or other variables (21).

Ratioing has been used successfully to identify areas of limonitic rocks in Land-

sat images (23). Sequential ratioing of the four MSS bands (1), 4/5, 5/6, and 6/7, results in black-and-white ratio images that can be optically combined to produce a color-ratio composite. Landsat color-ratio composites have proved valuable in differentiating among geologic units in areas showing low contrast on conventional MSS color composites (23, 24).

Future advances will probably include combining different types of image data and applying image processing techniques to geophysical and geochemical data normally not acquired in image form (25). Digital processing is a powerful tool, and its capabilities have not yet been fully exploited in geologic remote sensing.

### Regional Structural Features

Landsat MSS images are especially suitable for studying the relationships between landforms and major structural features, because each image displays approximately 34,000 square kilometers with uniform illumination, and the scene contrast can be optimized through digital processing of the radiance values. Mosaics of MSS images can provide unique views of the structural configuration of entire continental masses. The importance of these synoptic views of structural interpretations is indicated by the large number of reported applications, a few of which are described below.

One of the most striking results of the analysis of Landsat MSS images has been the discovery of numerous, previously unmapped regional linear features in areas considered to be reasonably well mapped as well as in poorly mapped areas. These features, referred to as lineaments (26), are alignments of regional morphological features, such as streams, escarpments and mountain ranges, and tonal features that in many areas are the surface expressions of fracture or fault zones (27). The lengths of lineaments recognized in satellite images are in consonance with those of major faults, ranging widely from a few kilometers to hundreds of kilometers.

The development of the concept of plate tectonics has provided a unified global framework for understanding most of the earth's major geologic features and the occurrences of its resources. An excellent example of the resolution of tectonic problems arising from plate interactions by application of satellite remote sensing is the use of Landsat images along with earthquake data to deduce the relative motions of the Indian subcontinent and Eurasia

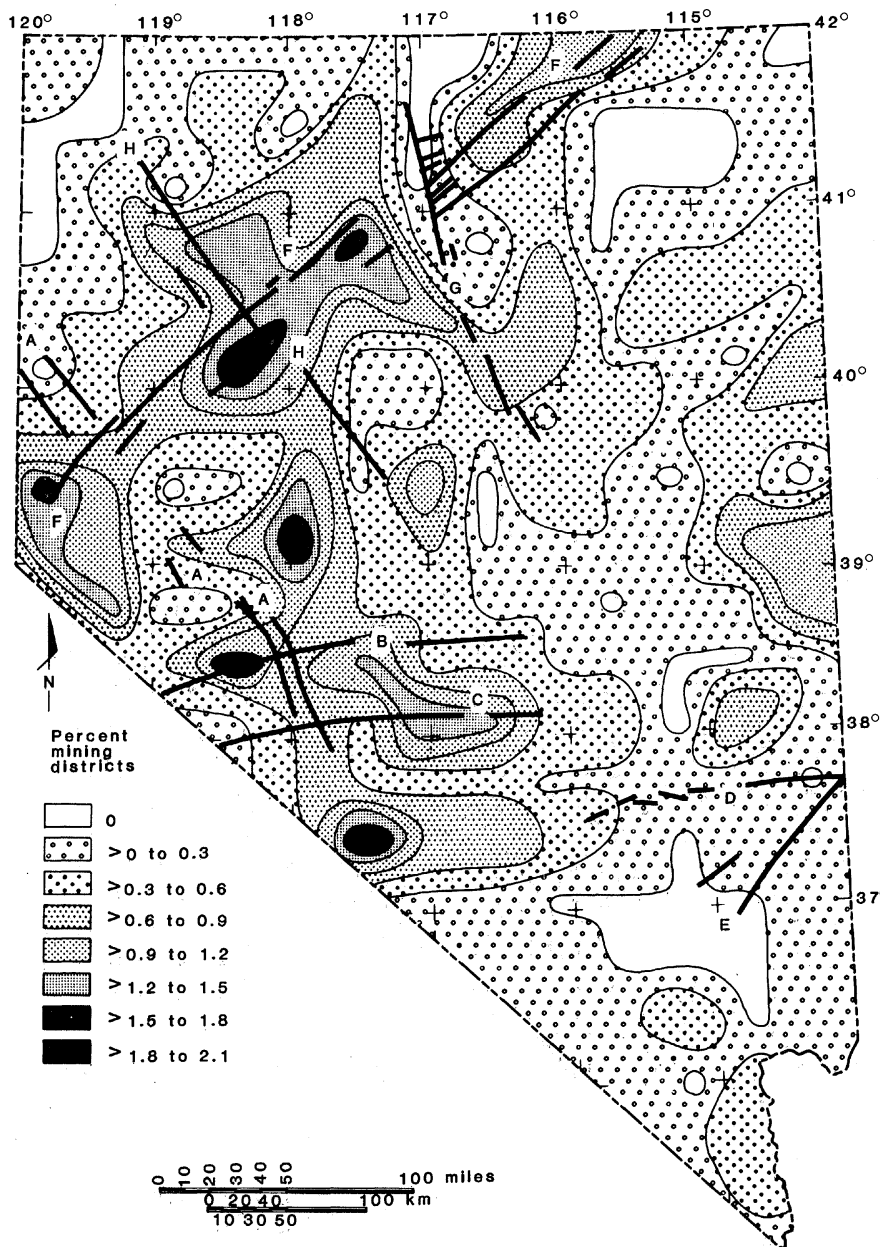


Fig. 5. Contour map of the areal density of metal-mining districts ( $N = 344$ ) in Nevada and the major lineament systems. Lineament A is located within the Walker Lane structural zone, lineament F lies within the Humboldt structural zone (44); and lineaments B, C, and D represent the southern Nevada structural zone; E locates the Pahrangat lineament system, and G locates the Northern Nevada Rift; H locates the Rye Patch lineament.

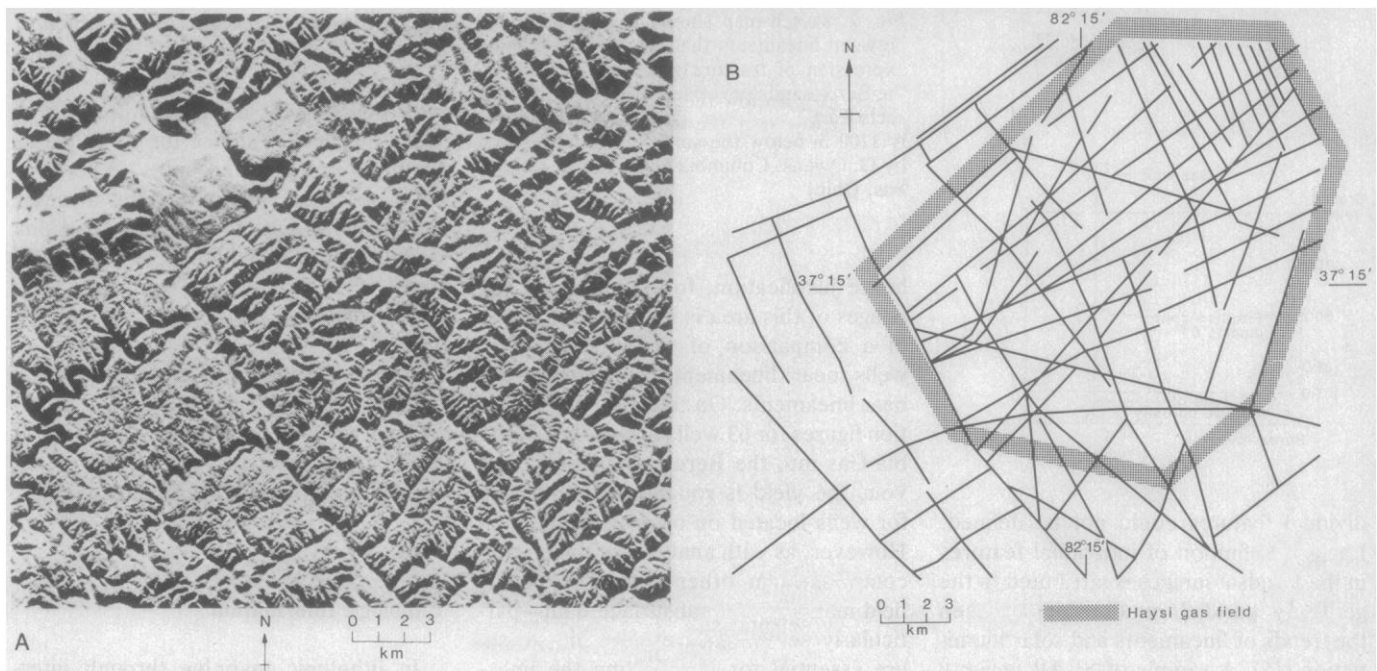


Fig. 6. (A) Side-looking radar (SLAR) image of the Haysi, Virginia-Kentucky gas field and (B) lineaments compiled from SLAR image by G. Owens, Columbia Gas System, Columbus, Ohio. [SLAR image acquired by Aero Service, Inc.]

(28). Extensive crustal deformation marked by earthquake activity was already recognized in Asia, but it was thought to be confined to a long, narrow zone and to be the result of enormous underthrusting of the Indian block beneath Eurasia. However, the regional distribution of landforms displayed in Landsat images supports the concept of deformation extending over a large area with as much as 1000 km of lateral movement along subparallel strike-slip faults (Fig. 4) similar to the San Andreas fault system. This interpretation is consistent with the broad distribution of earthquakes in Asia.

Lineaments are particularly important in mineral resource studies, because many, but not all, ore deposits are localized along fracture zones. In Nevada, for example, where mineral belts have been debated for many years (29, 30), six of the eight major lineaments delineated in Landsat images appear to represent three broader structural zones that have influenced the distribution of metal deposits (30) (Fig. 5).

Most of the metal districts are located within two of these broad zones: the Walker Lane structural zone and the Humboldt structural zone, expressed by lineaments A and F, respectively (Fig. 5). The Walker Lane zone was documented as a major zone of right-lateral strike-slip faults prior to the analysis of Landsat images (31), but the importance of east-trending structures in southern Nevada was first recognized when lineaments B, C, and D (Fig. 5) were found to

be coincident with similarly trending faults, volcanic features, and concentrations of ore deposits (30). In northern Nevada, several very long northeast-trending lineaments (F in Fig. 5) reflect the presence of the Humboldt structural zone. The deformed nature of this zone (100 to 200 km wide) is strongly indicated by the concentration of northeasterly oriented faults, and the broad crustal significance is supported by a transition in the gravity and magnetic fields and by the presence of the largest regional heat flow anomaly in the coterminous United States (30). Metal districts are clearly concentrated along the Humboldt zone in northern Nevada. Conversely, metal deposits are notably lacking along one of these linear features (E in Fig. 5) and the Northern Nevada Rift (32) (G in Fig. 5); these findings emphasize the importance of other factors in ore deposition and the need for integrating lineament analysis with conventional field mapping, geophysical data, and regional geochemical studies.

Several factors influence the detection of lineaments (33). One of the most important factors is the angular relationship between the linear feature and the illumination source. In general, features that trend parallel to the illumination source are not detected as readily as those that are oriented perpendicularly. Moreover, moderately low illumination angles are preferred for the detection of subtle topographic linear features. Because the Landsat satellites are in a sun-synchronous polar orbit, the only choice of illu-

mination that is available in a specific area stems from seasonal variations. Although these variations are important, some features are not well displayed in Landsat images and the lineament data set is biased.

Side-looking radar (SLAR) imaging systems provide a means of overcoming limitations due to solar illumination, because SLAR images are formed by transmitting bursts of energy to the surface and recording the returned signal on film or digital tape. The azimuth and illumination angle depend on the "look direction" and "look angle" of the system. A Columbia Gas System study by Owens and Ryan in 1975 illustrates the usefulness of SLAR images for delineating fracture zones in the Haysi, Virginia-Kentucky gas field. This field is situated on the rugged Allegheny Plateau in a zone of northwest-trending faults that mark the northeastern termination of the major Pine Mountain overthrust. Gas production from relatively tight sandstone formations is common in the Appalachian Basin, but the most productive wells are known to be located where the sandstone is naturally fractured. Ryan and Owens (34) concluded from an evaluation of several types of images, including Landsat images, black-and-white infrared, color, and color-infrared photographs and thermal-infrared and SLAR images, that the SLAR images recorded from several look directions were superior for mapping the individual lineaments. Although the general fault zone was visible as a lineament in Landsat images, in-

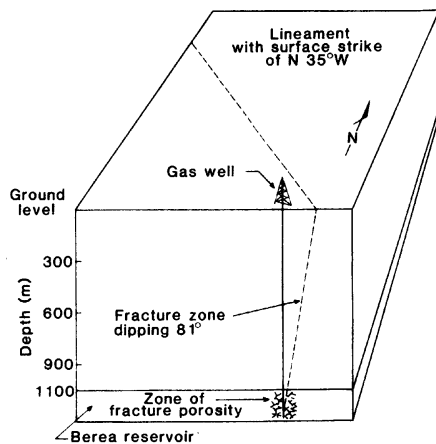


Fig. 7. Sketch map showing the relationship between lineaments that are the topographic expression of fracture zones that extend to the Berea sandstone reservoir. The well intersects fractured reservoir rock at approximately 1200 m below the surface. [Map prepared by G. Owens, Columbia Gas System, Columbus, Ohio]

dividual features could not be defined. Lack of definition of individual features in the Landsat images is attributed to the generally parallel relationship between the trends of lineaments and solar illumination (35). A sample of SLAR imagery of the Haysi area is shown in Fig. 6A. In Fig. 6B, note the concentration of north-westerly oriented lineaments which represent fractures at the termination of the Pine Mountain overthrust. Although the fracture zones are steeply dipping, wells must be located somewhat off the lineament in order to intersect the fractured reservoir approximately 1200 meters below the surface (Fig. 7).

The acquisition and processing of SLAR images is relatively expensive when compared with data such as Landsat images that are already available. However, the economic importance, and

hence justification, for acquiring SLAR images of this area is illustrated in terms of a comparison of the production of wells near lineaments with those not near lineaments. On the basis of production figures for 63 wells drilled by Columbia Gas into the Berea sandstone reservoir, the yield is roughly twice as high for wells located on or near lineaments. However, as with analyses of lineaments compiled from other types of images, field mapping and subsurface data—particularly seismic surveys in this case—are essential for interpreting the lineament data and understanding the regional tectonic framework. Because of the relatively high cost of SLAR data, the flight parameters, including flight direction, depression angle, and wavelength, must be carefully tailored for structural grain, topographic relief, and vegetation cover characterizing each study area. The SLAR images are particularly useful for studying continually cloud-covered areas (36).

This and other lineament studies in densely vegetated areas (16, 37) illustrate the value of the approach to geologic problems in areas of poor as well as good

rock exposures. Because of the difficulty of observing faults directly in the field, lineament analysis, used in conjunction with geophysical data, commonly provides the best evidence for some major fractures in vegetated areas. Where locally observed faults lie along a major lineament, a fault of regional proportions is indicated. Coincidence of these features with geophysical anomalies suggests projection of the features into the subsurface. Lineament analyses of Landsat, SLAR, and thermal-infrared images are therefore being applied to petroleum (38, 39), uranium (40, 41), geothermal (39), mineral (30, 42, 43), and several environmental problems (37, 44, 45).

#### Lithologic Information

In lithologic mapping through interpretation of Landsat images, several types of images are used, each of which is digitally processed to enhance the most diagnostic properties. In the visible and near-infrared regions, the most diagnostic properties of rocks are brightness (average reflectance in the visible and near-infrared regions), spectral radiance, and the spatial distribution of landforms. Brightness differences shown in conventional black-and-white photographs and single Landsat MSS bands allow discrimination of some units, but more separation is usually achieved if one analyzes color-composite images which in-

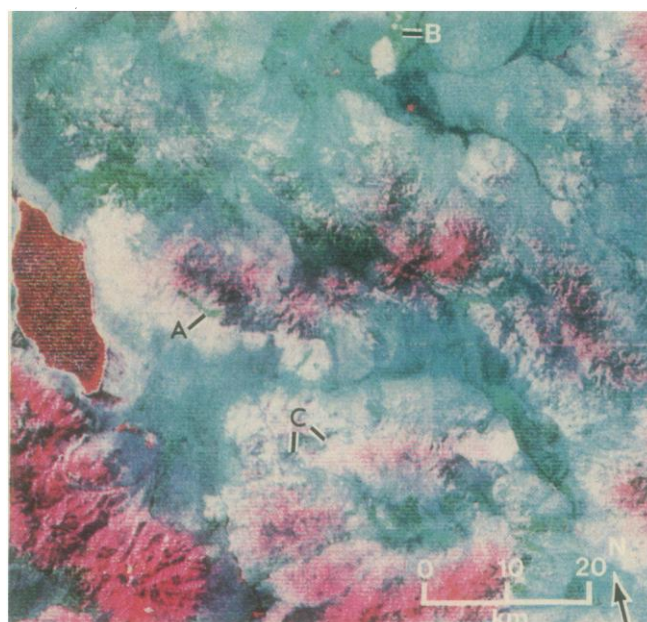
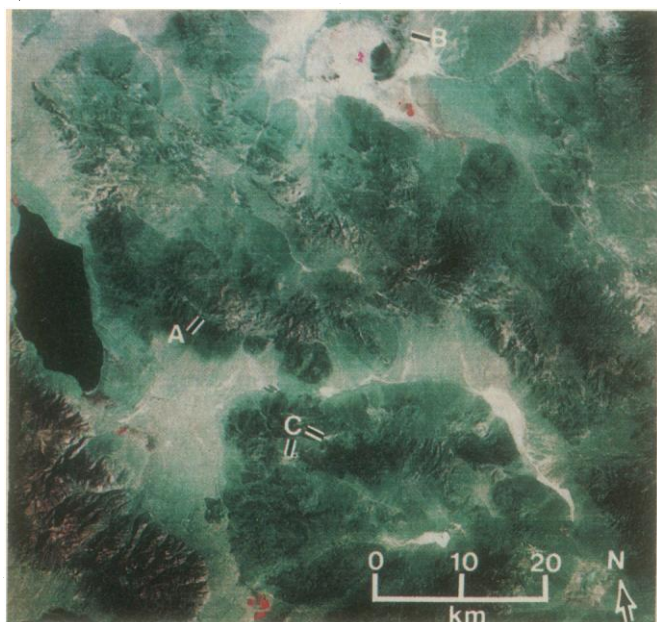


Fig. 8 (left). Section of a color-additive composite Landsat image of the Walker Lake, Nevada, area made from MSS bands 4, 5, and 7; A, limonitic, hydrothermally altered rocks; B, limonitic unaltered rocks; C, nonlimonitic altered rocks. [Image identification No. E2951-17293, EROS Data Center, Sioux Falls, South Dakota] Fig. 9 (right). Color-ratio composite Landsat image of the area shown in Fig. 8. Green areas in this image represent limonitic rocks. [Image produced by G. L. Raines, U.S. Geological Survey, Denver, Colorado]

corporate three spectral bands (Fig. 8) and hence display spectral radiances. Landsat color-infrared composite images consisting of MSS bands 4, 5, and 7 are widely used for lithologic as well as structural studies, because they present information about the brightness and spectral reflectance of rocks and landforms. In the color-infrared composite image (Fig. 8), dark rocks (mainly basic volcanic flows and scattered sedimentary rocks) and a wide range of bright rock types are readily separated. However, color differences, representing spectral reflectance variations, are very subtle, except for the red resulting from the high reflectance of vegetation in MSS band 7 relative to MSS bands 4 and 5 (Fig. 2). Another complicating factor is that the radiance variations are primarily related to changes in the topographic slope.

Color-ratio composite images are used to display spectral reflectance differences in color while subduing brightness variations due to topographic slope (Fig. 9) (9, 23, 46). A map showing the regional distribution of limonitic rocks is compiled by extracting the green areas from the image (Fig. 9). In large regions where limonite is nearly everywhere associated with altered rocks, regional maps of altered rocks can be prepared for roughly 10 percent of the costs of conventional methods (47). The technique is limited to regions having no more than 35 to 40 percent vegetation cover (48), but the acid soil conditions that characterize many hydrothermally altered areas tend to limit the vegetation cover. Furthermore, the MSS band passes impose two other important limitations: (i) limonitic hydrothermally altered rocks and limonitic unaltered rocks, such as those shown at points A and B, respectively, in Figs. 8 and 9, are not separable; and (ii) nonlimonitic hydrothermally altered rocks, such as those at point C in Figs. 8 and 9, are not detectable (9, 49). In areas where these problems are widespread, the cost benefit of this approach to mapping hydrothermally altered rocks declines. However, as we describe below, these problems can be largely overcome if one analyzes multispectral images recorded at longer wavelengths.

Mineral evaluations are significantly improved if one uses lineament and altered rock distributions together and then combines these data with geophysical and geochemical data. This approach has proved to be very successful for evaluating a 52,000-km<sup>2</sup> area in northern Sonora, Mexico. Because only reconnaissance geologic maps were available

and accessibility was difficult, analysis of lineaments and limonitic occurrences as seen in Landsat images was used initially to identify promising areas for more detailed geologic mapping and geochemical surveys (42).

Statistical analysis of mapped lineaments indicated the presence of two significant trends, northeast and north-northwest. Four northeast-trending lin-

eamment zones have been defined and are interpreted to be structural zones that controlled mineralization in the porphyry copper deposits of northern Sonora (Fig. 10) (42). Although northwest-trending structures also appear to have influenced the localization of ore deposits, these are pervasive structures that are not useful as regional prospecting guides. In contrast, the northeast-trend-

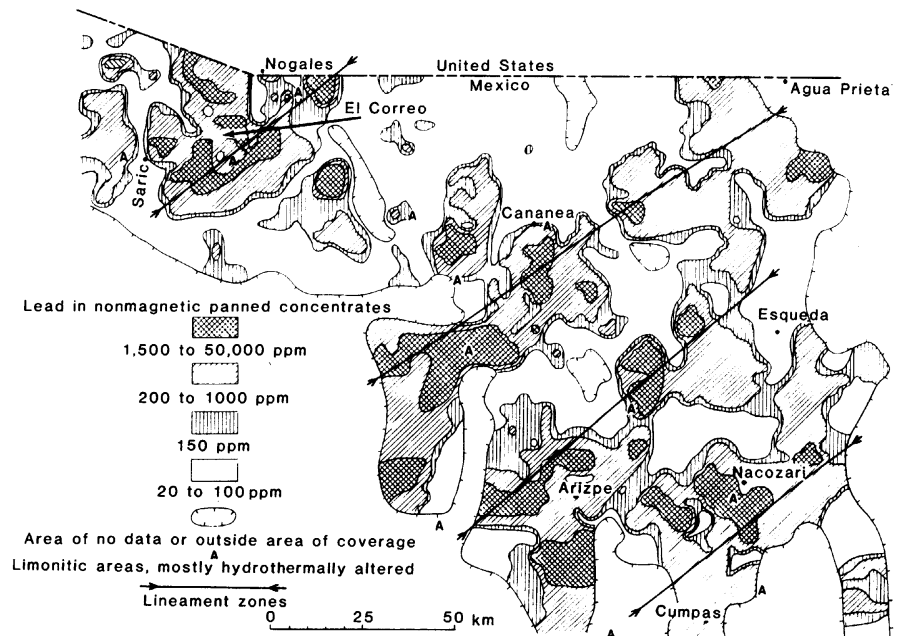
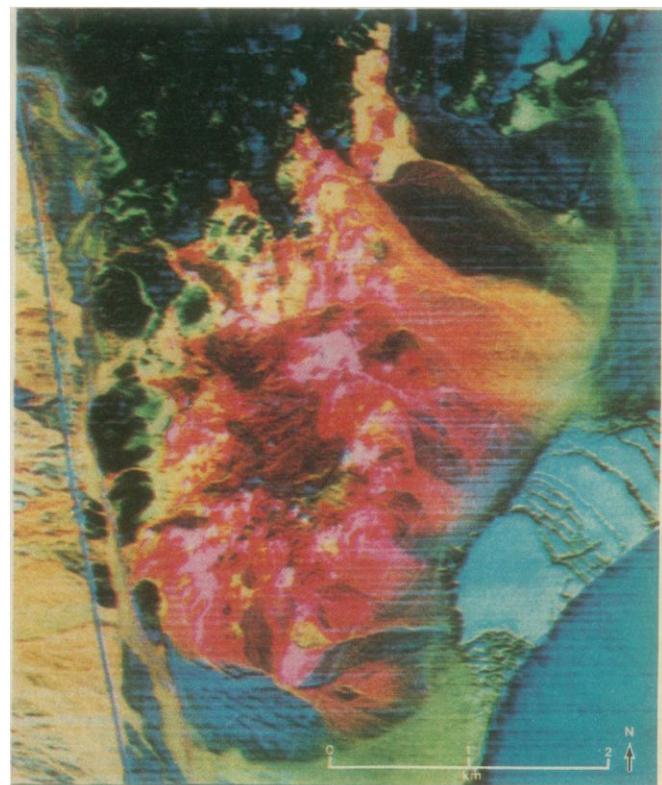


Fig. 10. Map of the northern Sonora, Mexico, area showing regional correlation among northeast-trending lineament zones (heavy lines), limonitic, hydrothermally altered rocks (A), and distribution of lead in stream sediments (41).

Fig. 11. Color-ratio composite NASA aircraft image of the Cuprite, Nevada, mining district. The following band ratios and color combinations are used: 1.6/0.48 as green, 1.6/2.2 as red, and 0.6/1.0 as blue (49). Red and magenta indicate intense absorption centered near 2.2  $\mu\text{m}$  due to the presence of kaolinite and alunite in opalized rocks; green, limonitic rocks; dark blue to black, spectrally flat rhyolite flows and tuffs and highly silicified, goethite-coated rocks; yellowish green, limonitic altered rocks with kaolinite.



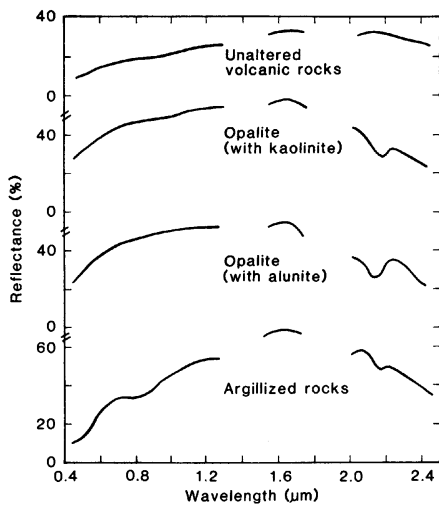
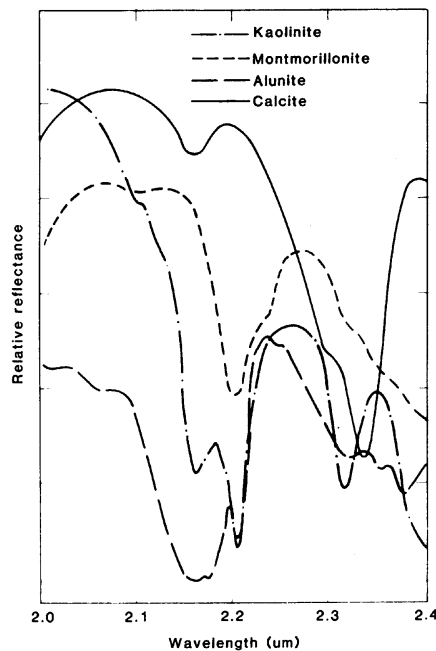


Fig. 12 (left). Representative spectral reflectance curves of altered and unaltered rocks in the Cuprite, Nevada, mining district (49). Fig. 13 (right). High-resolution laboratory reflectance spectra in the region from 2.0 to 2.4  $\mu\text{m}$  for some typical hydrothermal alteration minerals (55).



ing lineament zones are localized and associated with concentrations of limonitic, hydrothermally altered rocks (A in Fig. 10), occurrences of known copper deposits, and anomalously high lead content in stream sediment. These data along with other geochemical and geophysical data have resulted in the identification of several specific areas that appear to have exceptional economic potential.

### Geobotanical Information

Some geobotanical associations are related to regional lithologic variations, whereas others, such as barren areas and certain herbs and shrubs, are specifically related to anomalous concentrations of metals (50). Prior to the launch of Landsat-1, relatively small areas characterized by anomalous vegetation were mapped by means of aerial photographs and field studies. The availability of the multispectral, synoptic MSS images makes the study of regional geobotanical associations practical. Landsat MSS images have also been used successfully to detect barren areas associated with known metal concentrations (51).

One of the most interesting geobotanical applications of Landsat MSS images was conducted in the Powder River Basin, Wyoming, a region of significant uranium potential (41). The uranium deposits occur at boundaries between unoxidized gray and oxidized yellowish-gray sandstone with zones of red altered sandstone situated higher in the altered rock sequence. Although MSS color-ratio composite images accurately delineated areas of exposed limonitic rocks, limonitic materials that are not hydrothermally altered were not consistently distinguished from the limonitic altered rocks. Examination in the field was necessary to achieve this separation. A more severe problem was obscuration of many mineralized areas by vegetation, chiefly high prairie sage, grass, and herbs, that covers 50 to 75 percent of the ground (41).

A color-coded MSS 5/6 ratio image was used to display regional variation in the vegetation cover because this ratio is



Fig. 14. Principal component color-composite image of the central part of the East Tintic Mountains, Utah, made from multispectral mid-infrared NASA aircraft data (14, 61): A, quartz-rich rocks; B, interlayered quartz-rich and carbonate rocks; C, silicified rocks; D, quartz latite and quartz monzonite; E, latite and monzonite; and F, areas that exceeded the thermal response range of the scanner.

particularly sensitive to the proportions of vegetation, rock, and soil. In this image, Raines and his associates were able to show a spatial correlation between moderate vegetation cover and rocks having an intermediate ratio of sandstone to mudstone with which the uranium deposits are associated. This information along with structural information derived from lineament analysis led to the formulation of a model for the deposition of uranium in the Powder River Basin (41).

One of the more promising experiments in the application of remote-sensing techniques to mineral exploration uses very high resolution spectra from aircraft recorded in the region from 0.45 to 0.95  $\mu\text{m}$  to detect a slight ( $\sim 15$  nanometers) shift in band position in the reflectance of vegetation growing in areas with anomalous metal content (52). The most important shift occurs toward shorter wavelengths on the shoulder from 0.70 to 0.75  $\mu\text{m}$  of the chlorophyll *a* absorption band centered near 0.68  $\mu\text{m}$ . In the study area, Cotter Basin, Montana, a zone of veins containing copper and lead sulfide minerals was detected by wave-form analysis of the spectra recorded along closely spaced flight lines (53). It is especially encouraging that these 1976 results were repeated in 1978. Their repeatability strongly suggests that the vegetation anomalies probably persist with time. Much more research is needed, however, to establish the uniqueness of this shift in vegetation spectra, to determine the effects of seasons, sun angle, precipitation, and environmental factors, and to gain a better understanding of the phenomenon.

## Recent Results from Aircraft

### Experiments

The contribution of remote sensing to the geologic process will become more significant as lithologic determination is improved. As noted earlier, considerably more compositional information can be obtained if one analyzes multispectral data recorded at longer wavelengths than the Landsat MSS bands. Evaluations of field spectra and multispectral aircraft images show that bandpasses centered near 1.6 and 2.2  $\mu\text{m}$  are especially useful for mapping altered rocks, because  $\text{OH}^-$ -bearing minerals, commonly contained in these rocks, give rise to a relatively sharp absorption band near 2.2  $\mu\text{m}$  and a decrease in reflectance associated with the 2.74- $\mu\text{m}$   $\text{OH}^-$  absorption. The 2.2- $\mu\text{m}$  band is either absent or weak in the spectra for most unaltered regional lith-

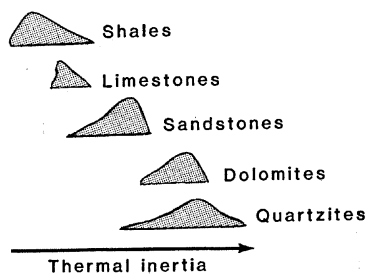


Fig. 15. Typical variation of thermal inertia values for sedimentary rocks (65).

ologic units in arid and semiarid environments (Fig. 2).

Color-ratio composite images made from National Aeronautics and Space Administration (NASA) aircraft data that include bandpasses centered at 2.2 and 1.6  $\mu\text{m}$  illustrate that bleached, non-limonitic altered rocks in the Cuprite, Nevada, mining district, which were not identified in Landsat MSS images, are correctly categorized (Fig. 11) (49). Colors in the image can be related to the spectral characteristics of the rocks in the district (Fig. 12).

In an identical color-ratio composite of the Coaldale, Nevada, area, limonitic unaltered tuffs were readily identified by their green color, indicating limonite but no  $\text{OH}^-$ -bearing minerals (54). These rocks were inseparable from limonitic altered rocks in MSS color-ratio composite images (9). The Landsat MSS does not record data in the 2.2- and 1.6- $\mu\text{m}$  regions. However, these bandpasses will be included in the Landsat D Thematic Mapper system scheduled to be launched in 1982. Analysis of these data should allow resolution of most of the ambiguities in the mapping of altered rocks with Landsat MSS images.

Detailed examination of reflectance spectra for hydrothermally altered rocks containing  $\text{OH}^-$ -bearing mineral shows that the minima near 2.2  $\mu\text{m}$  shift as a function of the composition (Fig. 12). High-resolution laboratory spectra (Fig. 13) indicate that important mineralogical information can be gained if one exploits this wavelength region (55). In order to test this approach to remote mineralogical determination, the Shuttle Multispectral Infrared Radiometer (SMIRR) was constructed to be flown on board the second space shuttle flight (56).

Another technique, the spectral emittance approach to identifying rock types, has not been adequately tested from orbital altitudes, but a series of aircraft experiments have shown the importance of this technique (14, 57). The most encouraging results thus far are in the analysis of multispectral mid-infrared aircraft im-

ages of the central part of the East Tintic Mountains, Utah (14). This area is particularly challenging for lithologic determinations by remote sensing because a variety of rock types, including Paleozoic quartzite, shale, carbonate rocks, and Tertiary extrusive and intrusive rocks of felsic to intermediate composition, are present (58). Several types of hydrothermally altered rocks are also present, with argillized and silicified rocks being the most widespread (54, 58, 59). In addition, vegetation cover and topographic relief are moderately high (48, 60).

A principal component color-composite image (Fig. 14) derived from three spectral bands in the region from 8.3 to 9.8  $\mu\text{m}$  exhibits red to pink, green, and blue colors primarily (14, 61). In general, the red colors represent rocks in which quartz is a major component, and green indicates nonsilicate rocks (limestone and dolomite) and vegetation (61). These results indicate that very important lithologic information can be obtained in bandpasses that do not include the 9.6- $\mu\text{m}$  ozone absorption band (Fig. 1). Ozone has been considered to be a limiting factor in multispectral mid-infrared imaging from orbit.

Because both vegetation and nonsilicate rocks are green in this image, a visible and near-infrared color-ratio composite image must be used to separate these two materials (59). This image must also be used in conjunction with the color mid-infrared image to distinguish between silicified and argillized altered rocks. These results illustrate the importance of multispectral mid-infrared images but also stress the value of these data when used in combination with the visible and near-infrared portions of the spectrum.

The use of the parameter thermal inertia, which characterizes the response of rocks and soils to diurnal heating and cooling, has been demonstrated from satellites with the use of Nimbus 3 and Nimbus 4 data (62), as well as from aircraft altitudes (6, 63). Because thermal inertia is a body property, some distinctions are possible that cannot be obtained from spectral reflectance and emittance data alone. For example, limestone and dolomite are readily separable on the basis of the significantly higher thermal inertia (63) of dolomite, even though these rocks are essentially spectrally similar in the mid-infrared and the visible and near-infrared regions (13, 64). In general, this technique is especially effective for distinguishing among sedimentary rocks (Fig. 15) (65). Thermal inertia studies complement the spectral approaches.

## Future Directions

The main contributions of remote-sensing information to the geologic mapping process will continue to be in the areas of morphology, structure, and lithologic mapping. Landsat has laid the groundwork for the widespread use of synoptic image data for regional structural interpretation. Landsat images have also reopened an old controversy concerning the origin and importance of lineaments, the large throughgoing fractures seen on almost any scene. Questions abound concerning the age of these crustal features, their vertical extent, and their importance as conduits for magma and ore fluids. These questions are related to more general problems in plate tectonics concerning the history of plate movement, the dynamical interaction of crustal blocks, and the driving forces. Although much has been learned about the present state of the crust and mantle by geophysical methods, in particular seismology, the history of most of the past events is finally recorded on the surface of the earth. Remote sensing is a powerful technique with which to unravel this history.

There still remains much virgin territory in geologic remote sensing that will require new instruments and techniques with which to explore. Some of the approaches to be taken include the following:

1) Global stereoscopic image coverage with resolution five or more times greater than Landsat to derive dips of strata, aid in landform interpretation, and reveal evidence for faults.

2) High-spectral-resolution imaging in the region from 2 to 2.5  $\mu\text{m}$  for the identification of layered silicates, clays, and carbonates.

3) Exploitation of the region from 8 to 14  $\mu\text{m}$  through multispectral scanners, active laser spectral reflectance measurements, and orbiting high-spatial-resolution, broadband imagers.

4) Multifrequency and multipolarization radar systems for increased recognition of lithologic units based on surface roughness characteristics.

5) Active imaging systems in the near- and short-wavelength infrared region, utilizing tunable laser systems to obtain data in very narrow spectral bands not otherwise obtainable with passive systems. Active systems also have potential for obtaining elevation data directly without the aid of stereoscopic images.

Remote-sensing techniques alone cannot solve geologic problems. Neither can data taken in a single wavelength region. Data obtained at a particular spatial reso-

lution or coverage swath cannot contribute as much as a combination of data types. The future success of remote sensing will depend on understanding the value of each technique and integrating the various techniques into a geologic problem-solving methodology. Conversely, new tools will require new insights in geologic thinking and model development in order that we might best exploit them.

## References and Notes

1. Landsat refers to a group of three satellites launched sequentially beginning in July 1972. Each satellite contains two imaging systems, a Return Beam Vidicon (RBV) and a Multi-spectral Scanner (MSS). The discussions in this article refer to the MSS data only. The MSS is an optomechanical scanner covering a sub-spacecraft swath 185 km wide in four spectral channels in the region from 0.5 to 1.1  $\mu\text{m}$ . The spectral bands, designated 4, 5, 6, and 7, cover the regions 0.5 to 0.6, 0.6 to 0.7, 0.7 to 0.8, and 0.8 to 1.1  $\mu\text{m}$ , respectively. The data are transmitted to the earth in digital form from a sun-synchronous orbit at an altitude of 918 km. Each satellite obtains repeat coverage of the earth every 18 days. Data in the form of photographic and digital tape can be purchased from the Earth Resources Observation Satellite (EROS) Data Center, Sioux Falls, S.D. *Landsat Data Users Handbook* (U.S. Geological Survey, Sioux Falls, S.D., 1979).
2. M. J. Grolrier and W. C. Overstreet, *U.S. Geol. Surv. Misc. Invest. Ser. Map 11143-B* (1978).
3. R. G. Burns, *Mineralogical Applications of Crystal Field Theory* (Cambridge Univ. Press, London, 1970).
4. G. R. Hunt, *Geophysics* **42**, 501 (1977).
5. F. J. Janza, *Manual of Remote Sensing* (American Society of Photogrammetry, Falls Church, Va., 1975), chap. 4.
6. K. Watson, *Int. Workshop Earth Resour. Surv. Syst.* **7**, 409 (1971); *J. Geophys. Res.* **78**, 5904 (1973); L. C. Rowan, T. W. Offield, *Proc. 7th Int. Symp. Remote Sensing Environ.* **3**, 2017 (1971); K. Watson, *Proc. IEEE* **63**, 128 (1975); A. B. Kahle, A. R. Gillespie, A. F. H. Goetz, *Geophys. Res. Lett.* **3**, 26 (1976); A. B. Kahle, *J. Geophys. Res.* **82**, 1673 (1977); A. R. Gillespie and A. B. Kahle, *Photogramm. Eng. Remote Sensing* **43**, 983 (1977).
7. Charge-transfer absorption bands in minerals normally found in the ultraviolet are caused by the migration of electrons between neighboring metal ions. Electronic transitions generally create weaker absorption bands at longer wavelengths and are the result of changes from one energy level to another. In transition elements, the outermost electrons principally determine the location of the energy levels (4).
8. An altered rock is a rock that has undergone changes in its chemical and mineralogical structure since its original deposition. Hydrothermal alteration is due to interaction with aqueous solutions heated by magma, that is, hydrothermal solutions or fluids.
9. L. C. Rowan, A. F. H. Goetz, R. P. Ashley, *Geophysics* **42**, 522 (1977).
10. A bending-stretching vibrational mode is created by the interaction of the fundamental OH stretching vibration at 2.74  $\mu\text{m}$  and the Al-OH or Mg-OH bending fundamental. These vibrations create narrow bands that characteristically fall in the region from 2.1 to 2.4  $\mu\text{m}$  for micas, clays, and amphiboles.
11. W. A. Hovis, Jr., *Appl. Opt.* **5**, 245 (1966).
12. P. J. Launer, *Am. Mineral.* **37**, 764 (1952); R. J. P. Lyon, *Econ. Geol.* **60**, 715 (1965); G. R. Hunt and J. W. Salisbury, *U.S. Air Force Cambridge Res. Lab. Rep. AFCRL-TR-74-0625* (1974); *U.S. Air Force Cambridge Res. Lab. Rep. AFCRL-TR-76-0003* (1976).
13. G. R. Hunt and J. W. Salisbury, *U.S. Air Force Cambridge Res. Lab. Rep. AFCRL-TR-75-0356* (1975).
14. A. B. Kahle, L. C. Rowan, D. P. Madura, in *Proceedings of the Annual Meeting of the Geological Society of America* (Geological Society of America, Boulder, Colo., 1978), p. 431; A. B. Kahle and L. C. Rowan, *Geology* **8**, 234 (1980).
15. P. Hoekstra and A. Delaney, *J. Geophys. Res.* **79**, 1699 (1974); J. C. Blinn, J. E. Conel, J. G. Quade, *ibid.* **77**, 4366 (1972).
16. H. C. MacDonald, *Mod. Geol.* **1**, 1 (1969).
17. G. Schaber, G. L. Berlin, W. E. Brown, *Geol. Soc. Am. Bull.* **87**, 29 (1976); L. R. Baker and R. M. Scott, *Manual of Remote Sensing* (American Society of Photogrammetry, Falls Church, Va., 1975), chap. 7, p. 325; M. Daily, C. Elachi, T. Farr, G. Schaber, *Geophys. Res. Lett.* **5**, 889 (1978).
18. Skylab data are obtainable from the EROS Data Center, Sioux Falls, S.D.; *Skylab EREP [Earth Resources Experiment Package] Investigations Summary* (NASA Publication SP-399, NASA Johnson Space Center, Houston, Tex., 1978).
19. Seasat synthetic aperture radar data are obtainable from the Environmental Data and Information Service, Satellite Data Services Division, Room 606, World Weather Building, Washington, D.C.; G. H. Born, J. A. Dunne, D. B. Lame, *Science* **204**, 1405 (1979).
20. The HCMM data are obtainable from the National Space Science Data Center, Code 601.4, NASA Goddard Space Flight Center, Greenbelt, Md.; *Heat Capacity Mapping Mission User's Guide* (NASA Goddard Space Flight Center, Greenbelt, Md., 1978).
21. H. C. Andrews, *Introduction to Mathematical Techniques in Pattern Recognition* (Wiley-Interscience, New York, 1972); A. R. Gillespie, in *Remote Sensing in Geology*, B. S. Siegal and A. R. Gillespie, Eds. (Wiley, New York, 1980), chap. 6.
22. E. Yost, R. Anderson, A. F. H. Goetz, *Photogr. Sci. Eng.* **17**, 177 (1973).
23. L. C. Rowan, P. H. Wetlaufer, A. F. H. Goetz, F. C. Billingsley, J. H. Stewart, *U.S. Geol. Surv. Prof. Pap.* **883** (1974).
24. A. F. H. Goetz, S. C. Billingsley, A. R. Gillespie, M. J. Abrams, R. L. Squires, E. M. Shoemaker, I. Lucchitta, D. P. Elston, *Jet Propulsion Lab. Tech. Rep. 32-1597* (1975).
25. A. Missallati, A. E. Prelat, R. J. P. Lyon, *Remote Sensing Environ.* **8**, 189 (1979).
26. W. H. Hobbs, *Geol. Soc. Am. Bull.* **22**, 123 (1911); D. W. O'Leary, J. D. Friedman, H. A. Pohn, *ibid.* **87**, 1463 (1977); R. A. Hodgson, in *Proceedings of the First International Conference on the New Basement Tectonics*, R. A. Hodgson et al., Eds. (Basement Tectonics Committee, Denver, 1976), p. 1.
27. Y. Isachsen, in *Proceedings of the Symposium on Management and Utilization of Remote Sensing Data* (American Society of Photogrammetry, Falls Church, Va., 1973), p. 342; E. B. Ekren, R. C. Bucknam, W. J. Carr, G. Dixon, W. D. Quinnlivan, *U.S. Geol. Surv. Prof. Pap.* **986** (1976); H. C. MacDonald and R. S. Grubbs, in *Proceedings of the NASA Earth Resources Survey Symposium* (NASA Publication TM X-58168, National Aeronautics and Space Administration, Washington, D.C., 1975), vol. 1, p. 769; M. R. Canich and D. P. Gold, in *Proceedings of Second International Conference on the New Basement Tectonics* (Basement Tectonics Committee, Denver, 1979), p. 14.
28. P. Molnar and P. Tappanier, *Science* **189**, 419 (1975); *Sci. Am.* **236**, 30 (April 1977).
29. R. J. Roberts, *Nev. Bur. Mines Rep.* **13** (1966), p. 47; J. A. Nobel, *Geol. Soc. Am. Bull.* **81**, 1607 (1970); R. C. Horton, *Nev. Bur. Mines Rep.* **13** (1966), part A, p. 109; D. R. Shawe and J. H. Stewart, *Trans. AIME* **260**, 225 (1976); P. W. Guild, *J. Geol. Soc. London* **135**, 355 (1978); L. C. Rowan and P. H. Wetlaufer, *U.S. Geol. Surv. Type III Final Report NASA* (Publication NTIS E75-10386, National Technical Information Service, Springfield, Va., 1975).
30. L. C. Rowan and P. H. Wetlaufer, *U.S. Geol. Surv. Open File Rep.* **79-544** (1979).
31. J. H. Stewart, J. P. Albers, F. G. Poole, *Geol. Soc. Am. Bull.* **79**, 1407 (1968).
32. E. S. Robinson, *ibid.* **81**, 2045 (1970); M. L. Zoback and G. A. Thompson, *Geology* **6**, 111 (1978).
33. B. S. Siegal, *Mod. Geol.* **6**, 75 (1977).
34. W. M. Ryan and G. Owens, in *A Case History Research Conference* (Univ. of Kansas Press, Lawrence, 1975), p. 49.
35. G. Owens, personal communication.
36. R. S. Wing and H. C. MacDonald, *Am. Assoc. Pet. Geol. Bull.* **57**, 825 (1973).
37. A. J. Eggenberger, D. Rowlands, P. C. Rizzo, in *Proceedings of the NASA Earth Resources Survey Symposium* (NASA Publication TM X-58168, National Aeronautics and Space Administration, Washington, D.C., 1975), vol. 1-B, p. 799; P. M. Merfield and D. L. Lamar, in *ibid.*, p. 779; D. W. O'Leary, *Geophysics* **42**, 542 (1977); H. A. Pohn, M. H. Podwysocki, I. S. Merin, *Geol. Soc. Am. Meeting Abstracts Program Northeast. Sect.* (1979), p. 49; M. H. Podwysocki, H. Pohn, I. S. Merin, D. Krohn, J. D. Phillips, L. C. Rowan, in *ibid.*, p. 49.
38. J. R. Everett and G. Petzel, in *Third Earth Resources Technology Satellite Symposium*

- (NASA Publication SP-356, National Aeronautics and Space Administration, Washington, D.C., 1973), p. 50; F. P. Benz and S. I. Gutman, *U.S. Geol. Surv. Prof. Pap. 1015* (1977), p. 83; J. B. Miller, in *Proceedings of the NASA Earth Resources Survey Symposium* (NASA Publication TM X-58168, National Aeronautics and Space Administration, Washington, D.C., 1975), vol. 1-B, p. 605; E. A. Latham, L. L. Talleur, W. W. Patton, Jr., in *Symposium on Significant Results Obtained from ERTS-1 [Earth Resources Technology Satellite]* (NASA Publication SP-327, National Aeronautics and Space Administration, Washington, D.C., 1973), vol. 1, section A, p. 257; N. M. Short, in *Remote Sensing Applications for Mineral Exploration*, W. L. Smith, Ed. (Dowden, Hutchinson, & Ross, Stroudsburg, Pa., 1977), p. 251.
39. F. F. Sabins, Jr., *Remote Sensing, Principles and Interpretation* (Freeman, San Francisco, 1978).
  40. B. C. Salmon and W. W. Pillars, *Environ. Res. Inst. Mich. Rep. 110400-2-F* (1975); T. W. Offield, in *Exploration of Uranium Ore Deposits* (International Atomic Energy Agency, Vienna, 1976), p. 731.
  41. G. L. Raines, T. W. Offield, E. S. Santos, *Econ. Geol.* **73**, 1706 (1978).
  42. G. L. Raines, P. K. Theobald, M. D. Kleinkopf, J. L. Moreno, M. F. de la Fuente Duch, in *Programs and Abstracts, International Association on the Genesis of Ore Deposits, 5th Symposium* (Lehigh University, Bethlehem, Pa., 1978), p. 148; G. L. Raines, *U.S. Geol. Surv. J. Res.* **6**, 51 (1978).
  43. T. W. Offield *et al.*, *Geophysics* **42**, 482 (1977).
  44. J. D. Friedman and S. L. Simpson, *U.S. Geol. Surv. Open-File Rep. 78-900* (1978).
  45. T. W. Offield, *Geol. Soc. Am. Bull.* **86**, 495 (1975).
  46. R. K. Vincent, in *Remote Sensing Applications for Mineral Exploration*, W. L. Smith, Ed. (Dowden, Hutchinson, & Ross, Stroudsburg, Pa., 1977), p. 251.
  47. Hydrothermally altered rocks (8) are used as key surface indicators in the exploration for base and precious metals. L. C. Rowan, A. F. H. Goetz, R. P. Ashley, *NASA Type II Progress Report* (Publication NTIS E77-10047, National Technical Information Service, Springfield, Va., 1977).
  48. L. C. Rowan and M. J. Abrams, *U.S. Geol. Surv. Open-File Rep. 78-736* (1978); B. S. Siegal and A. F. H. Goetz, *Photogramm. Eng. Remote Sensing* **43**, 191 (1977).
  49. M. J. Abrams, R. P. Ashley, L. C. Rowan, A. F. H. Goetz, A. B. Kahle, *Geology* **5**, 736 (1977).
  50. R. R. Brooks, *Geobotany and Biogeochemistry in Mineral Exploration* (Harper & Row, New York, 1972); G. L. Raines and F. C. Canney, in *Remote Sensing in Geology*, B. S. Siegal and A. R. Gillespie, Eds. (Wiley, New York, 1980), chap. 12.
  51. B. Bølviken, F. Honey, S. R. Levine, R. J. P. Lyon, A. Prelat, *J. Geochem. Explor.* **8**, 457 (1977).
  52. H. Y. Chiu and W. Collins, *Photogramm. Eng. Remote Sensing* **44**, 507 (1978).
  53. W. Collins, G. L. Raines, F. C. Canney, in *Programs and Abstracts, International Association on the Genesis of Ore Deposits, 5th Symposium* (Lehigh University, Bethlehem, Pa., 1978), p. 74; W. Collins and H. Y. Chiu, in *Proceedings of the 1979 International Symposium on Remote Sensing of the Environment* (University of Michigan, Ann Arbor, in press).
  54. M. Abrams and R. Ashley, personal communications.
  55. G. R. Hunt and R. P. Ashley, *Econ. Geol.* **74**, 1613 (1979).
  56. A. F. H. Goetz, *Shuttle Multispectral Infrared Radiometer (SMIRR) Experiment Description* (Jet Propulsion Laboratory, Pasadena, Calif., in press).
  57. R. K. Vincent and F. Thomson, *J. Geophys. Res.* **77**, 2465 (1972); \_\_\_\_\_, K. Watson, *ibid.*, p. 2473; R. J. P. Lyon, *Science* **175**, 983 (1972).
  58. H. T. Morris, *U.S. Geol. Surv. Bull. 1142-K* (1964); *U.S. Geol. Surv. Bull. 1142-L* (1964); T. S. Lovering, *Econ. Geol. Monogr. 1* (1949); H. T. Morris and T. S. Lovering, *U.S. Geol. Surv. Prof. Pap. 1024* (1979).
  59. L. C. Rowan and M. J. Abrams, in *Programs and Abstracts, International Association on the Genesis of Ore Deposits, 5th Symposium* (Lehigh University, Bethlehem, Pa., 1978), p. 156.
  60. H. T. Morris and T. S. Lovering, *U.S. Geol. Surv. Prof. Pap. 361* (1961); N. M. Milton and D. P. Madura, *U.S. Geol. Surv. Misc. Field Stud. Map 1195* (1980).
  61. A. B. Kahle, D. P. Madura, J. M. Shoa, *Jet Propulsion Lab. Publ. 79-80* (1979).
  62. H. A. Pohn, T. W. Offield, K. Watson, *U.S. Geol. Surv. J. Res.* **2**, 147 (1974).
  63. L. C. Rowan, T. W. Offield, K. Watson, P. J. Cannon, W. D. Watson, *Geol. Soc. Am. Bull.* **81**, 3549 (1970).
  64. G. R. Hunt and J. W. Salisbury, *Mod. Geol.* **2**, 195 (1971).
  65. K. Watson, in *Mathematical and Physical Principles of Research* (Centre Nationale d'Etude Spatiales, Strasbourg, France, 1979), p. 109.
  66. We are grateful to K. Watson and G. Raines of the U.S. Geological Survey and A. Kahle and J. Conel of the Jet Propulsion Laboratory for their constructive suggestions. This article is the result of research carried out at the Jet Propulsion Laboratory, California Institute of Technology, under contract NAS 7-100 sponsored by the National Aeronautics and Space Administration.

## AAAS-Newcomb Cleveland Prize

### To Be Awarded for an Article or a Report Published in *Science*

The AAAS-Newcomb Cleveland Prize is awarded annually to the author of an outstanding paper published in *Science* from August through July. This competition year starts with the 1 August 1980 issue of *Science* and ends with that of 31 July 1981. The value of the prize is \$5000; the winner also receives a bronze medal.

Reports and Articles that include original research data, theories, or syntheses and are fundamental contributions to basic knowledge or technical achievements of far-reaching consequence are eligible for consideration for the prize. The paper must be a first-time publication of the author's own work. Reference to pertinent earlier work by the author may be included to give perspective.

Throughout the year, readers are invited to nominate papers appearing in the Reports or Articles sections. Nominations must be typed, and the following information provided: the title of the paper, issue in which it was published, author's name, and a brief statement of justification for nomination. Nominations should be submitted to AAAS-Newcomb Cleveland Prize, AAAS, 1515 Massachusetts Avenue, NW, Washington, D.C. 20005. Final selection will rest with a panel of distinguished scientists appointed by the Board of Directors.

The award will be presented at a session of the annual meeting. In cases of multiple authorship, the prize will be divided equally between or among the authors.

-----  
Deadline for nominations: postmarked 15 August 1981

## Nomination Form

### AAAS-Newcomb Cleveland Prize

AUTHOR: \_\_\_\_\_

TITLE: \_\_\_\_\_

DATE PUBLISHED: \_\_\_\_\_

JUSTIFICATION: \_\_\_\_\_

\_\_\_\_\_  
 \_\_\_\_\_  
 \_\_\_\_\_  
 \_\_\_\_\_  
 \_\_\_\_\_  
 \_\_\_\_\_